Analysis of Photo-Irradiated Double-Drift Region Silicon Impact Avalanche Transit Time Devices in the Millimeter-wave and Terahertz Regime

Aritra Acharyya [1*] and J. P. Banerjee [1]
[1] Institute of Radio Physics and Electronics, University of Calcutta, 92, APC Road, Kolkata 700009, India.
[*1] E-mail: ari_besu@yahoo.co.in

(Received May 08 2012; accepted June 17 2012)

Abstract: Effect of photo-irradiation on the avalanche response time of Millimeter-wave (mm-wave) and Terahertz (THz) Double-Drift Region (DDR) Silicon Impact Avalanche Transit Time (IMPATT) devices is investigated in this paper. A model to study the photo-irradiation effect on the DC and high-frequency properties of the mm-wave and THz IMPATTs is developed by the authors based on which the simulation is carried out to calculate the avalanche response time of 94, 140, 220 *GHz* and 0.3 *THz* DDR Silicon IMPATTs under two different optical illumination configurations (Top Mount (TM) and Flip Chip (FC)). It is interesting to observe that the DC and high-frequency parameters of the device are more sensitive to electron dominated photo current (TM structure) compared to the hole dominated photo current (FC structure). Results show that the avalanche response time of the device decreases due to optical illumination on both TM and FC structures and percentage of decrease in avalanche response time in TM structure is higher as compared to that in FC structure. Larger decrement of avalanche response time due to optical illumination in TM structure causes larger deviation of phase shift between RF voltage and terminal current of the device from 180^0 which is the ideal phase difference between current and voltage for maximum RF power output; this is the main cause of greater reduction in RF power output in TM structure compared to FC structure due to optical illumination.

Keywords: Avalanche response time, DDR IMPATT device, Flip chip, Top mount, Terahertz regime.

doi: 10.11906/TST.097-113.2012.06.09

1. Introduction

Impact Avalanche Transit Time (IMPATT) device is the well established solid-state device to generate sufficiently high power in microwave, millimeter-wave and terahertz frequencies. Theoretical studies on IMPATT device were carried out by W. T. Read [1] in 1958 and his proposed IMPATT structure which is well known as Read structure. The high frequency performance of IMPATTs depends on material parameters (carrier ionization rates, drift velocities etc) of base semiconductor material [2]. The drift velocities of charge carriers (electrons and holes) in most semiconductors increase linearly with electric field at low-field range due to the acoustic phonon scattering. However, at higher fields ($\xi > 10^6$ *V/m*) the dominant scattering is due to optical phonons arising from high thermal vibrations of the lattice as a result of which the drift velocity of charge carriers saturates. Thus the transit time (τ_T) required by the charge carriers to cross the depletion region of IMPATT device is proportional to the depletion layer width, since the drift velocity is constant at higher field range. The avalanche response time [3] of the charge carriers (electrons and holes) is related to the avalanche multiplication process and plays an important role in determining the high frequency performance of the device. The photo irradiation on IMPATT devices leads to optical control of the high frequency properties of these devices. The optical control provides additional control over normal electronic control of the device and is of considerable research interest in view of its application in optoelectronic

integrated circuits and phased array antennas for space based communication and imaging. Several optical control functions of the photo-irradiated device such as modulation of RF power, frequency tuning, injection locking have already been theoretically and experimentally demonstrated [4-10]. The physical mechanism underlying these control functions is generation of photocurrent and consequent enhancement of leakage current in reverse biased device.

In this paper the authors have made an attempt to investigate the effect of optical illumination on the avalanche response time of the charge carriers (electrons and holes) in mm-wave and THz DDR Silicon IMPATT devices. A model to study the photo-irradiation effect on the DC and high-frequency properties of the mm-wave and THz IMPATTs is developed based on which the simulation is carried out to calculate the avalanche response time of 94, 140, 220 *GHz* and 0.3 *THz* IMPATTs under two different optical illumination configurations (Top Mount (TM) and Flip Chip (FC)). There are four very important frequencies, known as window frequencies (35, 94, 140 and 220 *GHz*) within the entire millimeter-wave range (30 – 300 *GHz*) where the atmospheric attenuation are lesser as compared to all other frequencies within this range. That's why in case of mm-wave communication systems, it is very much advantageous to choose any one of those window frequencies as carrier for transmission/reception purpose to achieve higher distance of coverage. This is the reason for which the mm-wave sources have to be designed to operate at any one of the atmospheric window frequencies as mentioned earlier. This is the primary reason for very high demand of research interests regarding those mm-wave windows. Another very important frequency is 300 *GHz* or 0.3 *THz* which is the starting threshold of the THz frequency regime (0.3 – 10 *THz*). That is why, in the present paper the authors have designed and studied the DDR Si IMPATT devices to operate at mm-wave windows (35 *GHz* frequency have been omitted from the present investigation, since lots of developments as regards sources, circuits and components have already achieved at this window frequency, which intern have lesser current research interest) and 0.3 *THz* frequency. Simulation is carried out by a well established indigenously built computer based device simulator [11-12] based on Gummel-Blue method [13] to obtain the DC and high frequency properties of the devices under consideration. We have obtained the DC and high frequency parameters of the DDR Si IMPATTs at 94, 140, 220 *GHz* and 0.3 *THz* only, under dark (unilluminated) and illuminated conditions. Graphs are plotted by joining point associated with those DC and high frequency parameters of DDR Si IMPATTs designed to operate at above mentioned frequencies by straight lines, since DC and high frequency parameters are not calculated for DDR Si IMPATT devices designed to operate at any frequency other than the previously mentioned frequencies. Actually the design and study of the IMPATT devices to operate at any frequency other than the previously mentioned frequencies are meaningless. Polynomial fitting may also be done to join the points, but it is not the extreme necessity since the authors' aim is to investigate the changes of DC and high frequency parameters due to photo irradiation on the device at the frequencies under consideration only.

2. Simulation method

One-dimensional model of reverse biased n^+npp^+ structure shown in Fig. 1 is used for DC and high frequency simulation of DDR IMPATT device.

A. DC Simulation

The DC electric field and current density profiles in the depletion layer of the device are obtained from simultaneous numerical solution of fundamental device equations i.e., Poisson's equation (equation (1)), combined carrier continuity equation in the steady state (equation (2)), current density equations (equations (3) & (4)) and mobile space charge equation (equation (5)) [14-15] subject to appropriate boundary conditions. A double iterative, field maximum simulation method based on Gummel-Blue approach [13] described elsewhere [11] is used to solve these equations and obtain the field and current density profiles. The above mentioned device equations are given by:

$$\frac{d\xi(x)}{dx} = \frac{q}{\varepsilon_s}\left(N_D - N_A + p(x) - n(x)\right) \tag{1}$$

$$\frac{\partial J_n(x)}{\partial x} = -\frac{\partial J_p(x)}{\partial x} = q\left(n(x)\alpha_n(x)v_n(x) + p(x)\alpha_p(x)v_p(x)\right) \tag{2}$$

$$J_p(x) = qp(x)v_p(x) - qD_P\left(\frac{\partial p(x)}{\partial x}\right) \tag{3}$$

$$J_n(x) = qn(x)v_n(x) + qD_n\left(\frac{\partial n(x)}{\partial x}\right) \tag{4}$$

$$q\frac{\partial(p(x)-n(x))}{\partial x} = J_0\left(\frac{\alpha_n(x)}{v_n(x)} + \frac{\alpha_p(x)}{v_p(x)}\right) - \left(\alpha_n(x) - \alpha_p(x)\right)\left(\frac{J_p(x)}{v_p(x)} - \frac{J_n(x)}{v_n(x)}\right)$$

$$+\left[J_p(x)\frac{\partial}{\partial\xi(x)}\left(\frac{1}{v_p(x)}\right) - J_n(x)\frac{\partial}{\partial\xi(x)}\left(\frac{1}{v_n(x)}\right)\right]\frac{\partial\xi(x)}{\partial x} \tag{5}$$

In the above mentioned simulation method, the computation starts from the field maximum near the metallurgical junction. The boundary conditions for the electric field at the depletion layer edges are given by:

$$\xi(-x_1) = 0 \qquad \text{and} \qquad \xi(x_2) = 0 \tag{6}$$

Similarly the boundary conditions for normalized current density $P(x) = (J_p(x) - J_n(x)) / J_0$ (where $J_0 = J_p + J_n$) at the depletion layer edges i.e., at $x = -x_1$ and $x = x_2$ are given by:

$$P(-x_1) = \left(\frac{2}{M_p} - 1\right) \qquad \text{and} \qquad P(x_2) = \left(1 - \frac{2}{M_n}\right) \tag{7}$$

where M_n and M_p are the electron and hole multiplication factors whose values are of the order of $\sim 10^6$ under dark or un-illuminated condition of the device.

Electric field profiles and current profiles are obtained from the DC simulation. The breakdown voltage is calculated by integrating the spatial field profile over the total depletion layer width (W), i.e.:

$$V_B = \int_{-x_1}^{x_2} \xi(x)dx \tag{8}$$

And the avalanche voltage is calculated by integrating the spatial field profile over the total avalanche layer width (x_A), i.e.:

$$V_A = \int_{-x_{A_1}}^{x_{A_2}} \xi(x)dx \tag{9}$$

Again the DC to RF conversion efficiency is calculated from the semi quantitative formula [16]:

$$\eta(\%) = \frac{2m}{\pi} \times \frac{V_D}{V_B} \tag{10}$$

where $V_D = (V_B - V_A)$ = voltage drop across the drift region and $m = 1/2$.

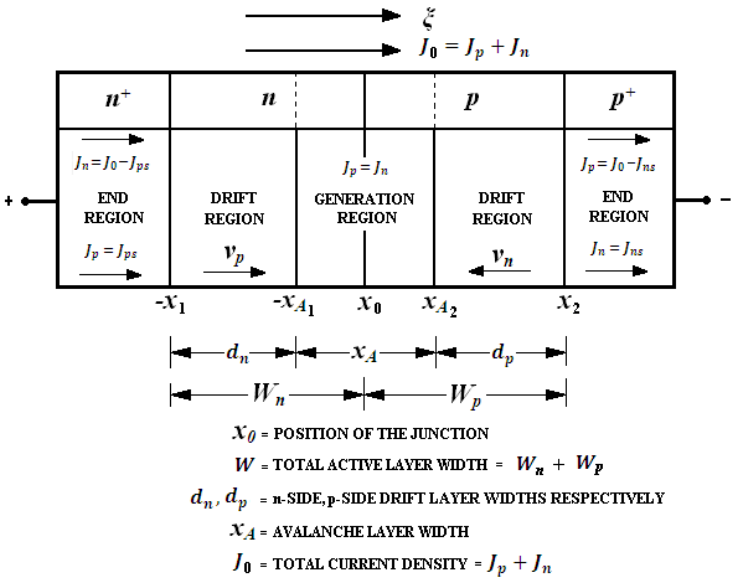

Fig. 1 One-dimensional model of DDR IMPATT device.

B. High frequency simulation

The magnitude of peak field at the junction (ξ_p), the widths of avalanche and drift zones (x_A and x_D; where $x_D = d_n + d_p$) and the voltage drops across these zones (V_A, V_D) are obtained from double-iterative simulation program. These values are fed back as input parameters in the high frequency simulation to obtain the admittance properties of the device. The depletion layer edges of the device obtained from the output of DC simulation program are taken as the starting and end points of numerical computation in the high frequency program. Two second order differential equations are framed by resolving the device impedance $Z(x,\omega)$ into its real part $R(x,\omega)$ and imaginary part $X(x,\omega)$; where, $Z(x,\omega) = R(x,\omega) + jX(x,\omega)$. Under small-signal condition the differential equations involving negative specific resistance R and specific reactance X are given by [12]:

$$D^2R + [\alpha_n(x) - \alpha_p(x)]DR - 2\underline{r}\left(\frac{\omega}{\underline{v}}\right)DX + \left[\left(\frac{\omega^2}{\underline{v}^2}\right) - H(x)\right]R - 2\underline{\alpha}(x)\left(\frac{\omega}{\underline{v}}\right)X - 2\left(\frac{\underline{\alpha}(x)}{\underline{v}\varepsilon_s}\right) = 0 \tag{11}$$

$$D^2X + \left[\alpha_n(x) - \alpha_p(x)\right]DX + 2\underline{r}\left(\frac{\omega}{\underline{v}}\right)DR + \left[\left(\frac{\omega^2}{\underline{v}^2}\right) - H(x)\right]X + 2\underline{\alpha}(x)\left(\frac{\omega}{\underline{v}}\right)R + \left(\frac{\omega}{\underline{v}^2\varepsilon_s}\right) = 0 \tag{12}$$

where the following notations have been introduced, $\underline{v} = (v_{sn}v_{sp})^{0.5}$, $\underline{\alpha}(x) = (\alpha_n(x)v_{sn} + \alpha_p(x)v_{sp})/2\underline{v}$, $\underline{r} = (v_{sn} - v_{sp})/2\underline{v}$, $H(x) = (J_0/\underline{v}\varepsilon_s)[2d\underline{\alpha} / d\xi + y\, d(\alpha_n - \alpha_p)/d\xi]$, $H(x)$ is the linearization factor. $y = \underline{v}\varepsilon_s / J_0(d\xi_p/dx)$, ε_s = permittivity of the semiconductor, D is the differential operator $\partial/\partial x$.

The boundary conditions for R and X at the n^+n and p^+p interfaces are given by:

$$DR + \frac{\omega X}{v_{sn}} = -\left(\frac{1}{v_{sn}\varepsilon_s}\right) \text{ and } DX - \frac{\omega R}{v_{sn}} = 0 \qquad \text{at} \quad x = -x_1 \text{ i.e., at } n^+n \text{ interface} \tag{13}$$

$$DR - \frac{\omega X}{v_{sp}} = \left(\frac{1}{v_{sp}\varepsilon_s}\right) \text{ and } DX + \frac{\omega R}{v_{sp}} = 0 \qquad \text{at} \quad x = x_2 \quad \text{i.e., at } p^+p \text{ interface} \tag{14}$$

A double-iterative simulation over the initial choice of the values of R and X is described in details in [12] is used to solve simultaneously the two second order differential equations (11) and (12) in R and X subject to appropriate boundary conditions expressed in equations (13) and (14). The negative specific resistance ($R(x)$) and specific reactance ($X(x)$) profiles are obtained from the above solution. The device negative resistance (Z_R) and reactance (Z_X) are obtained from the numerical integration of the $R(x)$- and $X(x)$-profiles over the space-charge layer width (W) respectively, i.e.:

$$Z_R = \int_{-x_1}^{x_2} R(x)dx \qquad \text{and} \qquad Z_X = \int_{-x_1}^{x_2} X(x)dx \tag{15}$$

The impedance of the device is given by, $Z_D = Z_R + j\, Z_X$ and the device admittance is, $Y_D = 1/Z_D = G + j\, B$. The negative conductance (G) and positive susceptance (B) are computed from the following expressions:

$$|G(\omega)| = \frac{Z_R}{\left(Z_R^{\,2} + Z_X^{\,2}\right)} \qquad \text{and} \qquad |B(\omega)| = \frac{-Z_X}{\left(Z_R^{\,2} + Z_X^{\,2}\right)} \tag{16}$$

It may be noted that both G and B are normalized to the area of the diode. The admittance ($G(\omega)$ versus $B(\omega)$) plots of the device can be obtained for different bias current densities from the above analysis. The avalanche resonance frequency (f_a) is the frequency at which the susceptance (B) changes its nature from inductive to capacitive. Again it is the lowest frequency at which the real part (G) of admittance becomes negative and oscillation starts to build up in the circuit. The RF power output P_{RF} from the device can be obtained from the following expression given by:

$$P_{RF} = \frac{1}{2}(V_{RF})^2 |G_p| A_j \tag{17}$$

where V_{RF} is the RF voltage ($V_{RF} = m_x \times V_B$; m_x = 1/2 for 50 % voltage modulation), $|G_p|$ is the peak magnitude of the negative conductance at peak optimum frequency (f_p) and A_j is the device junction area.

C. Calculation of avalanche response time

If τ_{An} and τ_{Ap} be the avalanche response times initiated by electrons and holes respectively, then these are expressed as [3]:

$$\tau_{An} = \frac{1}{(v_{sn} + v_{sp})} \int_{-x_{A_1}}^{x_{A_2}} exp\left[- \int_{-x_{A_1}}^{x} (\alpha_n - \alpha_p) dx' \right] dx \tag{18}$$

$$\tau_{Ap} = \tau_{An} exp\left[\int_{-x_{A_1}}^{x_{A_2}} (\alpha_n - \alpha_p) dx \right] \tag{19}$$

When avalanche process is initiated by a mixture of electrons and holes then the corresponding response time τ_A is given by [3]:

$$\tau_A = \tau_{An} \left\{ (1-k) + k.exp\left[- \int_{-x_{A_1}}^{x_{A_2}} (\alpha_n - \alpha_p) dx \right] \right\}^{-1} \tag{20}$$

where the parameter $k = J_{ps}/J_s$ and $(1 - k) = J_{ns}/J_s$; $J_s = J_{ps} + J_{ns}$ is the total reverse saturation current of the device under dark condition.

3. Proposed model for analysis of IMPATT devices under optical illumination

The optical energy can be fed to the conventional vertical structure of DDR IMPATTs by shining light on either p^+-side (TM) or n^+-side (FC) of the ring contact of mesa device through a controlled optical window [4-6, 9] as shown in Fig. 2. In this section, a relationship between incident photon flux density and the normalized difference of electron and hole current density at the depletion layer edges is established. This relation is incorporated in the simulation program to study the effect of optical illumination for different incident photon flux density on the DC and high frequency properties of vertically oriented DDR Silicon IMPATT devices for operation at different mm-wave and THz frequencies.

If P_{in} watts of optical power is incident on the device having effective device illumination area of A, then the photon flux density Φ_0 is given by:

$$\Phi_0 = P_{in} \frac{(1 - R(\lambda))\lambda}{Ahc} \tag{21}$$

The electron-hole pair (EHP) generation rate due to optical illumination is given by:

$$G_L(x) = \Phi_0 \alpha(\lambda) exp(-\alpha(\lambda)x) = P_{in} \frac{\alpha(\lambda)(1 - R'(\lambda))\lambda}{Ahc} exp(-\alpha(\lambda)x) \tag{22}$$

where $\alpha(\lambda)$ and $R'(\lambda)$ are the absorption coefficient (m^{-1}) and reflectance [$R' = (n_2 - n_1)/(n_2 + n_1)$; n_2 = refractive index of the semiconductor, n_1 = refractive index of air] of the semiconductor material respectively at a wavelength of λ. The electron and hole multiplication factors at the n- & p-depletion layer edges are given by:

$$M_n = \frac{J_0}{J_{ns(Total)}} \qquad \text{and} \qquad M_p = \frac{J_0}{J_{ps(Total)}} \tag{23}$$

where $J_{ns/ps(Total)}$ is the total electron/hole reverse saturation current under optical illumination. Electron and hole reverse saturation currents can have two components, (a) thermally generated saturation currents, (b) optically generated saturation currents. Thus:

$$J_{ns(Total)} = J_{ns(Th)} + J_{ns(Opt)} \qquad \text{and} \qquad J_{ps(Total)} = J_{ps(Th)} + J_{ps(Opt)} \tag{24}$$

The expression for thermally generated electron and hole reverse saturation currents are given by:

$$J_{ns(Th)} = \left[\frac{qD_n {n_i}^2}{L_n N_A}\right] \qquad \text{and} \qquad J_{ps(Th)} = \left[\frac{qD_p {n_i}^2}{L_p N_D}\right] \tag{25}$$

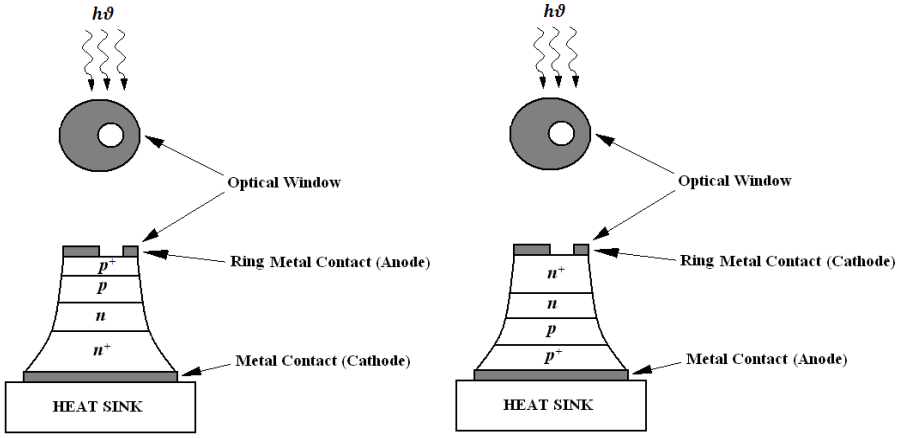

Fig. 2 Schematic diagram of (a) Top Mounted (TM) and (b) Flip Chip (FC) vertical DDR IMPATT structures under optical-illumination.

Under dark condition (i.e. when $J_{ns(Opt)} = J_{ps(Opt)} = 0$) both M_n and M_p remain in the order of ~10^6 [6]. The drift component of the photocurrent density through the reverse-biased depletion layer is given by:

$$J_{(Opt\_drift)} = -q\int_{-x_1}^{x_2} G_L(x)dx = qP_{in}\frac{\left(1-R'(\lambda)\right)\lambda}{A_j hc}\left\{exp(\alpha(\lambda)x_1) - exp(-\alpha(\lambda)x_2)\right\} \tag{26}$$

Due to very high conductivity, electric fields at the p^+- and n^+-layers are zero. Diffusion components of the photo current are generated within these undepleted p^+- and n^+-layers. Diffusion components of the photo current in both p^+- and n^+-layers separately can be determined by solving the one-dimensional diffusion equation with proper boundary conditions [17]. The electron and hole diffusion components of the photo current density in both p^+- and n^+-layers are given by:

$$J_{ns(Opt\_diff)} = qP_{in}\frac{(1-R(\lambda))\lambda}{A_j hc}\left(\frac{\alpha(\lambda)L_n}{1+\alpha(\lambda)L_n}\right)exp(-\alpha(\lambda)x_2) \tag{27}$$

$$J_{ps(Opt\_diff)} = qP_{in}\frac{(1-R(\lambda))\lambda}{A_j hc}\left(\frac{\alpha(\lambda)L_p}{1+\alpha(\lambda)L_p}\right)exp(-\alpha(\lambda)x_1) \tag{28}$$

Total photocurrent density is the combination of drift and diffusion components; i.e.:

$$\left.\begin{aligned} J_{ns(Opt)} &= J_{(Opt\_drift)} + J_{ns(Opt\_diff)} \\ \text{and} & \\ J_{ps(Opt)} &= J_{(Opt\_drift)} + J_{ps(Opt\_diff)} \end{aligned}\right\} \tag{29}$$

A. Top Mounted (TM) structure

In TM structure the light is shined on the p^+-side of the DDR IMPATT device. Thus the photocurrent density will be the electron dominated in an illuminated TM structure. So the electron and hole multiplication factors at the *n*- & *p*-depletion layer edges in illuminated TM structure are given by:

$$M_n' = \frac{J_0}{J_{ns(Th)} + J_{ns(Opt)}} \quad \text{and} \quad M_p = \frac{J_0}{J_{ps(Th)}} \tag{30}$$

In this case the value of M_n' is considerably reduced (<< 10^6) while M_p remains unchanged (~10^6). Thus the normalized current density boundary conditions at the depletion layer edges (equation (7)) are modified to:

$$P(-x_1) = -1 \quad \text{and} \quad P(x_2) = \left(1 - \frac{2}{M_n'}\right) \tag{31}$$

where M_p is very large (~10^6) and M_n' is much smaller than M_p. The equation (31) is used as one of the boundary conditions in the proposed model (in place of equation (7)) for simulating the DC and small-signal properties of the illuminated TM structure of DDR IMPATT device.

For the illuminated TM structure of DDR IMPATT device the value of *k* in the equation (20) can be written as:

$$k = \frac{J_{ps(Th)}}{J_{ps(Th)} + J_{ns(Th)} + J_{ns(Opt)}} \tag{32}$$

Thus the value of avalanche response time (τ_A) in illuminated TM structure will not remain same as the value of it in unilluminated device.

B. Flip Chip (FC) structure

In FC structure the light is shined on the n^+-side of the DDR IMPATT device. Thus the

photocurrent density will be the hole dominated in an illuminated FC structure. So the electron and hole multiplication factors at the *n*- & *p*-depletion layer edges in illuminated FC structure are given by:

$$M_n = \frac{J_0}{J_{ns(Th)}} \qquad \text{and} \qquad M_p{}' = \frac{J_0}{J_{ps(Th)} + J_{ps(Opt)}} \tag{33}$$

In this case the value of $M_p{}'$ is considerably reduced (<< 10^6) while M_n remains unchanged (~10^6). Thus the normalized current density boundary conditions at the depletion layer edges (equation (7)) are modified to:

$$P(-x_1) = \left(\frac{2}{M_p{}'} - 1 \right) \qquad \text{and} \qquad P(x_2) = 1 \tag{34}$$

where M_n is very large (~10^6) and $M_p{}'$ is much smaller than M_n. The equation (34) is used as one of the boundary conditions in the proposed model (in place of equation (7)) for simulating the DC and small-signal properties of the illuminated FC structure of DDR IMPATT device.

For the illuminated FC structure of DDR IMPATT device the value of k in the equation (20) can be written as:

$$k = \frac{J_{ps(Th)} + J_{ps(Opt)}}{J_{ps(Th)} + J_{ps(Opt)} + J_{ns(Th)}} \tag{35}$$

As a result, the value of avalanche response time (τ_A) in illuminated FC structure will not remain same as the value of it in unilluminated device. A complete list of symbols is given in Appendix 1, where each and every symbol is explained religiously.

4. Results and discussions

The active layer widths and background doping concentrations have been designed from a simple transit time formula given by $W_{n,p} = 0.37\ v_{sn,sp} / f_d$; where $W_{n,p}$, $v_{sn,sp}$ and f_d are the total depletion layer width (*n*- and *p*-side), saturation velocity of electrons and holes and design frequency respectively [18], so that the operating frequency of the devices remain nearly 94, 140, 220 *GHz* and 0.3 *THz*. The design parameters of DDR Silicon IMPATT devices are given in Table 1. Using a generalized computer method [11-12] based on Gummel-Blue approach [13] the DC and high frequency properties of the devices are obtained. Material parameters like ionization rates, saturation drift velocities and mobilities of electron and holes, dielectric constant, bandgap, absorption coefficient, diffusion coefficient, reflectance of the base semiconductor material (Si) used for the analysis are taken from [2, 19-21]. Simulated DC and high frequency parameters of the devices under dark condition are listed in Table 2 and Table 3 respectively.

Tab. 1 Doping and structural parameters.

BASE MATERIAL	SERIAL NUMBER	f_d (GHz)	W_n (μm)	W_p (μm)		N_D ($\times 10^{23}\ m^{-3}$)	N_A ($\times 10^{23}\ m^{-3}$)	N_{Sub} ($\times 10^{26}\ m^{-3}$)
Si	1	94	0.4000	0.3800		1.200	1.250	1.0
	2	140	0.2800	0.2450		1.800	2.100	1.0
	3	220	0.1800	0.1600		3.950	4.590	1.0
	4	300	0.1320	0.1120		6.000	7.300	1.0

Tab. 2 DC parameters of DDR Si IMPATTs under dark condition.

BASE MATERIAL	SERIAL NUMBER	J_0 ($\times 10^8\ Am^{-2}$)	ξ_p ($\times 10^7\ Vm^{-1}$)	V_B (V)	V_A (V)	η ($\%$)	x_A (μm)	x_A/W ($\%$)
Si	1	3.40	6.0115	24.27	16.21	10.58	0.352	46.32
	2	5.80	6.6617	18.98	13.52	9.16	0.268	53.07
	3	13.0	8.1990	13.74	10.29	7.99	0.170	53.10
	4	17.2	9.3490	11.29	9.07	6.25	0.134	59.82

Tab. 3 High frequency parameters of DDR Si IMPATTs under dark condition.

BASE MATERIAL	SERIAL NUMBER	f_p (GHz)	G_p ($\times 10^7\ Sm^{-2}$)	B_p ($\times 10^7\ Sm^{-2}$)	$Q = -(B_p/G_p)$	Z_R ($\times 10^{-9}\ \Omega m^{-2}$)	P_{RF}/A_j ($\times 10^9\ Wm^{-2}$)
Si	1	94	-4.0002	6.5654	1.64	-6.7679	2.9453
	2	140	-8.0772	15.4697	1.92	-2.6524	3.6372
	3	219	-18.0334	38.7885	2.15	-0.9855	4.2556
	4	302	-26.2239	80.1598	3.05	-0.3686	4.1783

Fig. 3 shows the variations of breakdown voltage and DC to RF conversion efficiency with peak optimum frequency of mm-wave DDR Si IMPATTs under dark ($\Phi_0 = 0$) and two optical illumination configurations (TM & FC) with incident photon flux density of $\Phi_0 = 10^{26}\ m^{-2}\ sec^{-1}$ of 1000 *nm* wavelength. It can be observed from Fig. 3 that both the breakdown voltage and efficiency of the device decreases due to the effect of optical illumination. Percentage of reduction in both these parameters is higher at higher frequencies for same incident photon flux density. It is interesting to observe that the reduction in breakdown voltage and efficiency of the device due to same degree of optical illumination (i.e. $\Phi_0 = 10^{26}\ m^{-2}\ sec^{-1}$ of 1000 *nm* wavelength) is higher in TM structure compared to the FC structure. The same nature can be observed from the Fig. 4 in which the peak negative conductances and the RF power output densities (P_{RF}/A_j) are plotted against peak operating frequencies of mm-wave and THz DDR Si IMPATTs. Photon flux density of $10^{26}\ m^{-2}$ sec^{-1} of 1000 *nm* wavelength causes a decrease of the magnitude of peak negative conductance and the RF power output density by 8.6% and 9.6% respectively for 94 *GHz* FC Structured DDR IMPATT and a decrease by 13.1% and 18.5% for 94 *GHz* TM Structured DDR IMPATT respectively. Similarly the same photon flux density leads to a decrease of the magnitude of peak negative conductance and the RF power output density by 20.4% and 29.9% for 0.3 *THz* FC Structured DDR IMPATT and a decrease by 30.5% and 45.0% for 300 *GHz* TM Structured DDR IMPATT respectively. Thus both the DC and small-signal parameters are more sensitive in electron dominated photo current (TM) compare to hole dominated photo current (FC). The cause of greater electron photo current sensitivity of Si IMPATTs is already explained in earlier papers [6-7, 22].

Avalanche response time of DDR IMPATTs operating at 94, 140, 220 *GHz* and 0.3 *THz* are calculated by using equation (20) under dark and two different optical illumination configurations (TM and FC). Variation of avalanche response time with operating frequency is plotted in Fig. 5. Avalanche response time of the device decreases significantly due to the effect of optical illumination. It can be noted from Fig. 5 that the effect of electron dominated photo current (TM)

on the avalanche response time of the device is more pronounced compared to hole dominated photo current (FC). For example 7.57% and 3.14% decrease in avalanche response time is observed in TM (electron dominated photo current) and FC (hole dominated photo current) structure of 94 *GHz* IMPATT respectively for the incident photon flux density of 10^{26} m^{-2} sec^{-1} at 1000 *nm* wavelength. Fig. 6 shows the variation of avalanche response time of illuminated 94 *GHz* DDR Si IMPATT device with incident photon flux density (λ = 1000 *nm*) under two optical illumination configurations (TM & FC). So it can be concluded that the avalanche response time of the device decreases as more number of photons are incident of the active layer of the device. Fig. 6 clearly shows that the reduction of avalanche response time greater when light is shined on the p^+-side of the device (i.e. in TM structure) compared to when the light is shined on the n^+-side of the device (i.e. in FC structure).

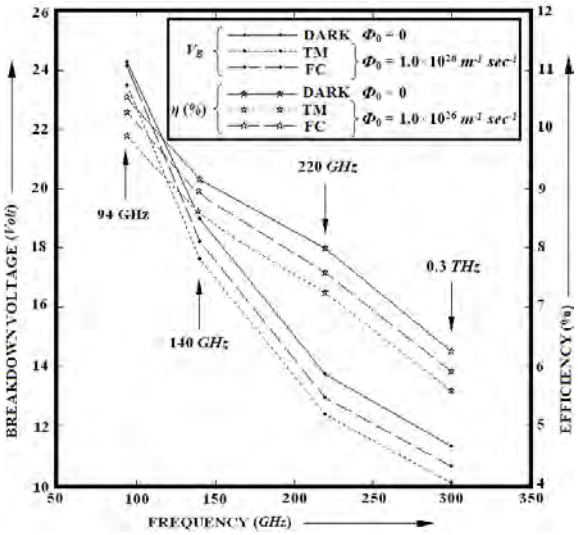

Fig. 3 Variations of breakdown voltage and DC to RF conversion efficiency with peak optimum frequency of mm-wave and THz DDR Si IMPATTs under dark and two optical illumination configurations (TM & FC) (λ =1000 *nm*).

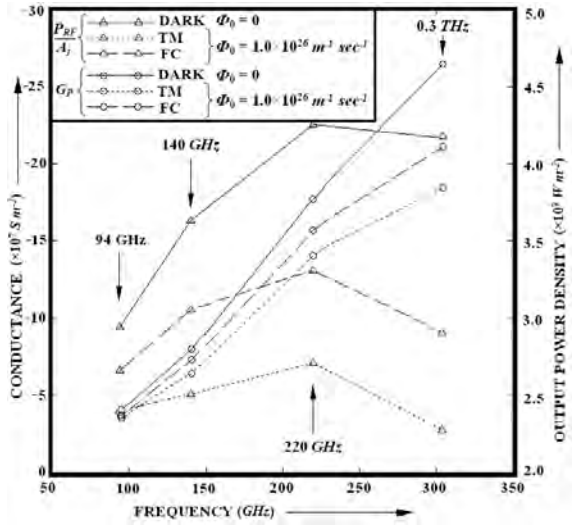

Fig. 4 Variations of output power density and peak negative conductance with peak optimum frequency of mm-wave and THz DDR Si IMPATTs under dark and two optical illumination configurations (TM & FC) (λ =1000 *nm*).

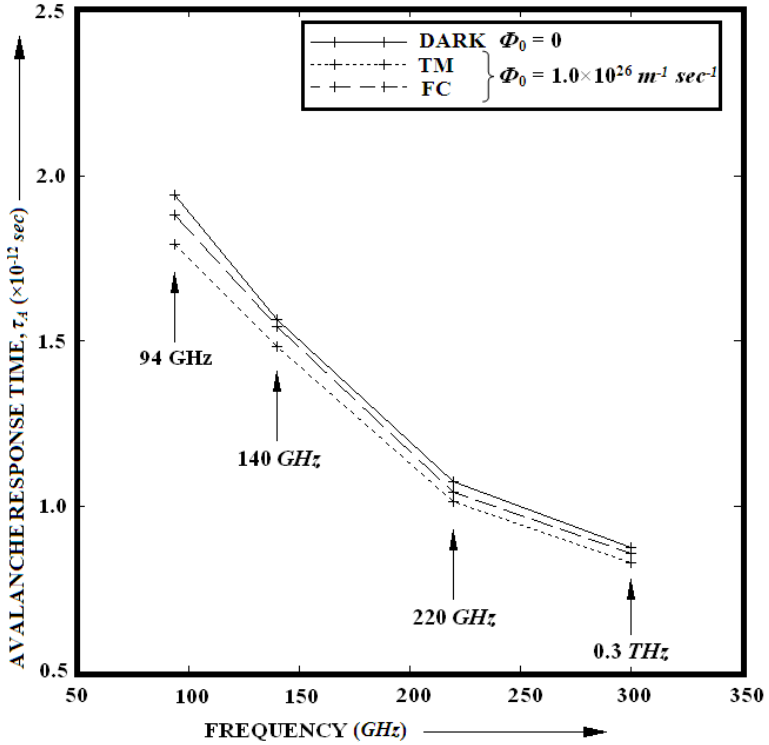

Fig. 5 Variations of avalanche response time with peak optimum frequency of mm-wave and THz DDR Si IMPATTs under dark and two optical illumination configurations (TM & FC) (λ =1000 *nm*).

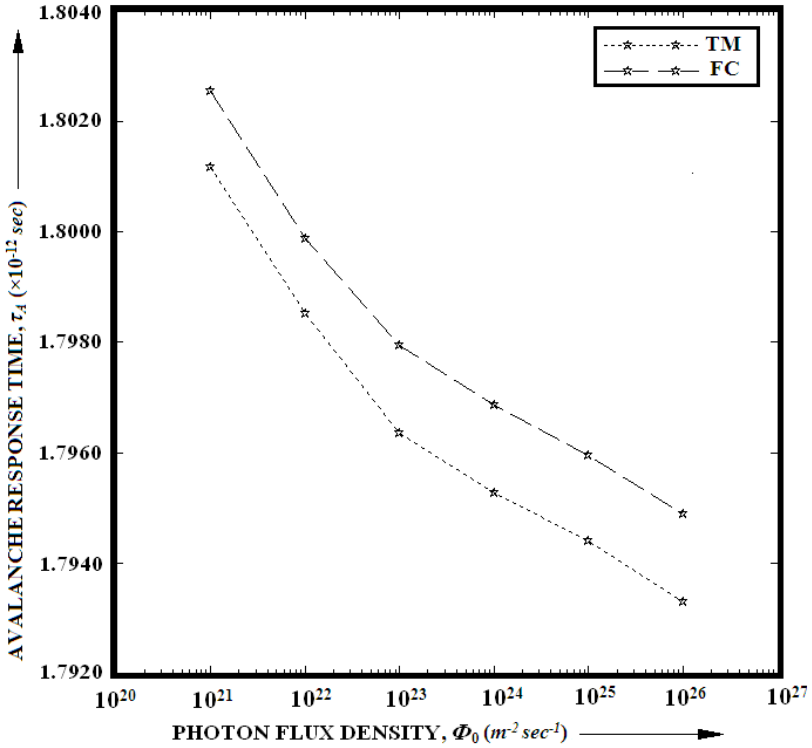

Fig. 6 Variation of avalanche response time with incident photon flux density (λ = 1000 *nm*) of illuminated 94 *GHz* DDR Si IMPATT under two optical illumination configurations (TM & FC).

5. Validation of the simulation results

There are many theoretical and experimental reports are available [3-10, 23] where the optical modulation of IMPATT devices is studied. But so far as authors' knowledge is concerned, there is no detailed theoretical investigation is available in published literatures which relate the incident optical flux to the changes in DC and high frequency properties of DDR IMPATT device due to optical illumination. In the present paper a simulation based model is developed to study the effect of incident photon flux density on the DC and high frequency properties of the DDR IMPATTs. The effect of optical illumination on the avalanche response time (which is the determining factor of the upper cut-off frequency limits of the IMPATT device based on a particular semiconductor; lower avalanche response time facilitates higher frequency of operation [3]) is investigated and it is interestingly observe that optical illumination causes decrease in avalanche response time thus the increase of peak operating frequency of the device. Also this study establishes the higher opto-sensitivity of TM structure as compared to FC structure. This same nature is already experimentally verified by several researchers [4-5, 9, 23]. Dependence of opto-sensitivity of electron or hole dominated photo current on the relative values of electron and hole ionization rates are already explained in the earlier papers [6-7]. Most of the experimental verifications of optical control of IMPATT devices are carried out for lower frequency bands (Microwave X-band). Only in [23] maximum operating frequency shift due to optical modulation in W-band (75-110 *GHz*) Si IMPATT is obtained as 9.4 *MHz* at 91.3 *GHz*; whereas in our case we have found the same as around 700 *MHz* at 94 *GHz*, which is in close agreement with the experimentally obtained result [23]. Slight deviation in the theoretical result from the experimental result may be due to the difference in structural and electrical bias conditions of the device and the intensity of the applied photon flux. But no experimental report on optical modulation of Si DDR IMPATTs is available for higher mm-wave and THz frequencies (> 94 *GHz*). That is why the simulation results presented in this paper could not be validated by experimentally obtained results for higher mm-wave and THz frequencies (> 94 *GHz*).

6. Conclusions

In this paper the authors have made an attempt to investigate the effect of photo-irradiation on the avalanche response time of mm-wave and THz DDR Si IMPATT devices. A model to analyze the effect of photo-irradiation on the DC and high-frequency properties of the mm-wave and THz IMPATTs is developed based on which the simulation is carried out to calculate the avalanche response time of 94, 140, 220 *GHz* and 0.3 *THz* DDR Si IMPATTs under two different optical illumination configurations (Top Mount (TM) and Flip Chip (FC)). It is interesting to observe that the DC and high-frequency parameters of the device are more sensitive to electron dominated photo current (TM structure) compared to the hole dominated photo current (FC structure). Results show that the avalanche response time of the device decreases due to optical illumination on both TM and FC structures. The percentage of decrease in avalanche response time in TM structure is higher compared to FC structure. For example 7.57% decrease in avalanche response time is observed in TM structure of 94 *GHz* IMPATT, whereas the same is only 3.14% in FC structure for the incident photon flux density of 10^{26} m^{-2} sec^{-1} at 1000 *nm* wavelength near band gap absorption of Silicon. Larger decrement of avalanche response time due to optical illumination in TM structure causes larger deviation of phase shift between RF voltage and terminal current of the device from 180^{o} which is the ideal phase difference between

current and voltage for maximum RF power output; this is the main cause of greater reduction in RF power output in TM structure compared to FC structure due to optical illumination which is clearly reflected in the simulation results.

Appendix 1: *List of Symbols*

A	Device illumination area
A_j	Device junction area
α	Absorption coefficient
$\alpha_{n,p}$	Electron and hole ionization rates
B	Device susceptance
B_p	Peak susceptance
c	Velocity of light in free space
D	Differential operator
$d_{n.p}$	*n*-side and *p*-side drift layer widths
$D_{n,p}$	Electron and hole diffusion coefficients
ξ	Electric field
ξ_p	Peak electric field near the metallurgical junction
ε_s	Permittivity of the semiconductor
f_d	Design frequency
f_p	Peak optimum frequency
Φ_0	Photon flux density
G	Device negative conductance
G_L	EHP generation rates
G_p	Peak negative conductance
h	Plank's constant
$J_{n,p}$	Electron and hole component of the bias current density
J_0	Bias current density
$J_{ns(Total)}$	Electron component of the total saturation current
$J_{ps(Total)}$	Hole component of the total saturation current
$J_{ns(Th)}$	Thermal component of the electron saturation current
$J_{ps(Th)}$	Thermal component of the hole saturation current
$J_{ns(Opt)}$	Total optically generated electron saturation current
$J_{ps(Opt)}$	Total optically generated hole saturation current
$J_{(Opt\_drift)}$	Total optically generated drift component of the saturation current
$J_{ns(Opt\_diff)}$	Optically generated diffusion component of the electron saturation current
$J_{ps(Opt\_diff)}$	Optically generated diffusion component of the hole saturation current
J_s	Total reverse saturation current under dark condition
$L_{n,p}$	Electron and hole diffusion lengths
λ	Wavelength

$M_{n,p}$	Electron and hole multiplication factors under dark condition
$M_n^{'}$	Electron multiplication factor in TM structure
$M_p^{'}$	Hole multiplication factor in FC structure
n	Electron concentration
n_1	Refractive index of air
n_2	Refractive index of semiconductor
n_i	Intrinsic carrier concentration
N_A	Acceptor concentration
N_D	Donor concentration
N_{Sub}	Doping concentrations of n^+- and p^+-layers
η	DC to RF conversion efficiency
p	Hole concentration
P_{in}	Input optical power
P_{RF}	RF power output
$P(x)$	Normalized current density parameter
q	Electronic charge
Q_p	Q-factor
R	Device specific resistance
$R^{'}$	Reflectance
τ_{An}	Avalanche response time initiated by electron
τ_{Ap}	Avalanche response time initiated by holes
τ_A	Avalanche response time initiated by mixture of electron and holes
τ_T	Transit time
$v_{n,p}$	Electron and hole drift velocities
$v_{sn,sp}$	Electron and hole saturated drift velocities
V_A	Avalanche voltage
V_B	Breakdown voltage
V_D	Total voltage drop across the drift layers
W	Total depletion layer width
$W_{n,p}$	n-side and p-side depletion layer widths
ω	Angular frequency
x	Spatial distance in the depletion layer
x_A	Avalanche layer width
x_D	Total drift layer width
X	Device specific reactance
V_{RF}	RF voltage
Z_R	Device negative resistance
Z_X	Device reactance

References

[1] W. T. Read, "A proposed high-frequency negative-resistance diode", *Bell Syst. Tech. J.*, 37, 401-466, (1958).

[2] "Electronic Archive: New Semiconductor Materials, Characteristics and Properties", http://www.ioffe.ru/SVA/NSM/Semicond/Si.html.

[3] A. Acharyya, S. Banerjee, and J. P. Banerjee, "Calculation of Avalanche Response Time for Determining the High Frequency Performance Limitations of IMPATT Devices", *Journal of Electron Devices*, 12, 756-760, (2012).

[4] H. P. Vyas, R. J. Gutmann, and J. M. Borrego, "Leakage current enhancement in IMPATT oscillator by photo-excitation", *Eletron. Lett.*, 13, 189-90, (1977).

[5] H. P. Vyas, R. J. Gutmann and J. M. Borrego, "Effect of hole versus electron photocurrent on microwave-optical interactions in impatt oscillators", *IEEE Transactions on Electron Devices*, 26(3), 232-34, (1979).

[6] A. Acharyya and J. P. Banerjee, "A Comparative Study on the Effect of Optical Illumination on $Si_{1-x}Ge_x$ and Si Based DDR IMPATT Diodes at W-Band", *Iranian Journal of Electronics & Electrical Engineering*, 7(3), 179-189, (2011).

[7] R. Mukherjee and J. P. Banerjee, "Effect of electron and hole dominant photocurrent on the millimeter-wave properties of Indium Phosphide Impatt diode at 94 GHz", *Semiconductor Science and Technology*, 9, 1-4, (1994).

[8] H. W. Yen, M. K. Barnoski, R. G. Hunsperger and R. T. Melville, "Switching of GaAs IMPATT diode oscillator by optical illumination", *Appl. Phys. Lett.*, 31, 120-121, (1977).

[9] A. Schweighart, A., H. P. Vyas, J. M. Borrego and R. J. Gutmann, "Avalanche diode structure suitable for microwave-optical interaction", *Solid-Sate Electron.*, 21, 1119-1121, (1978).

[10] J. R. Forrest and A. J. Seeds, "Optical injection locking of impatt oscillators", *Electronics Letters*, 14(19), 626-27, (1978).

[11] S. K. Roy, M. Sridharan, R. Ghosh, and B. B. Pal, "Computer methods for the dc field and carrier current profiles in impatt devices starting from the field extremum in the depletion layer", *Proc. of NASECODE-I Conf. on Numerical Analysis of Semiconductor Devices (Dublin: Boole Press)*, 266-274, (1979).

[12] S. K. Roy, J. P. Banerjee and S. P. Pati, "A computer analysis of the distribution of high frequency negative resistance in the depletion layers of impatt diodes", *Proc. of NASECODE-IV Conf. on Numerical Analysis of Semiconductor Devices (Dublin: Boole Press)*, 494-500, (1985).

[13] H. K. Gummel and J. L. Blue, "A small-signal theory of avalanche noise in IMPATT diodes", *IEEE Trans. on Electron Devices*, 14(9), 569-580, (1967).

[14] M. Sridharan and S. K. Roy, "Computer studies on the widening of the avalanche zone and decrease on efficiency in silicon X-band sym. DDR", *Electron Lett.*, 14, 635-637, (1978).

[15] M. Sridharan and S. K. Roy, "Effect of mobile space charge on the small signal admittance of silicon DDR", *Solid State Electron*, 23, 1001-1003, (1980).

[16] D. L. Scharfetter and H. K. Gummel, "Large-Signal Analysis of a Silicon Read Diode Oscillator", *IEEE Trans. on Electron Devices*, 16(1), 64-77, (1969).

[17] S. M. Sze and Kwok K. Ng, *Physics of Semiconductor Devices*, Willy India, 2010.

[18] S. M. Sze and R. M. Ryder, "Microwave Avalanche Diodes", *Proc. of IEEE, Special Issue on Microwave Semiconductor Devices*, 59(8), 1140-1154, (1971).

[19] W. N. Grant, "Electron and hole ionization rates in epitaxial Silicon", *Solid State Electron*, 16, 1189-1203, (1973).

[20] C. Canali, G. Ottaviani and A. A. Quaranta, "Drift velocity of electrons and holes and associated anisotropic effects in silicon", *J. Phys. Chem. Solids*, 32(8), 1707, (1971).

[21] B. Van Zeghbroeck, *Principles of Semiconductor Devices*, Colorado Press, (2011).

[22] J. P. Banerjee R. Mukherjee, J. Mukherjee and P. N. Mallik, "Studies on Avalanche Phase Delay and the Admittance of an Optically Illuminated Indium Phosphide Avalanche Transit Time Diode at Millimeter Wave Window Frequencies", *Phys. Stat. Sol. (a)*, 153(2), 567-579, (1996).

[23] A. J. Seeds, A. Augusto, "Optical control of microwave semiconductor devices", *IEEE trans. on Microwave Theory and Techniques*, 38(5), 577-585, (1990).